MODERN ASTRONOMY: FROM THE EARLY UNIVERSE TO EXOPLANETS AND BLACK HOLES

Radial profiles of systematic velocities in massive protostellar cores

L. Pirogov and P. Zemlyanukha

Gaponov-Grekhov Institute of Applied Physics of the Russian Academy of Sciences,
46 Ul'yanov str., Nizhny Novgorod, 603950 Russia

Abstract. The knowledge of systematic velocity radial profiles in the star-forming cores is important for theoretical models. We analyzed the HCO^+(1–0) spectral maps of five massive cores from the MALT90 database associated with the regions of high-mass star formation at different stages of evolution. We fitted the maps calculated in the framework of spherically symmetric model into observed ones. An approach based on the principal component analysis and the k-nearest neighbors method was used to find minimum of the error function between model and observed spectral maps. Radial profiles of density, turbulent and systematic velocity are obtained. Densities in the cores decrease with radial distance with power-law indices ranging from 1.5 to 2.5, turbulent velocities decrease with power-law indices ranging from 0.3 to 0.45. Systematic (infall) velocity profiles in the cores are close to $r^{-0.1}$ which differs from what is expected for free fall. Analysis of the ^{13}CO (2–1) SEDIGISM data for three sample objects has revealed the V-shape features on the position-velocity profiles which implies motions from surrounding gas to the cores. Taken together, the results support the scenario of globally contracting cores which interact with their surroundings.

Keywords: stars: formation, dense cores; methods: laboratory: molecular, modelling

DOI: 10.26119/VAK2024.082

1 Introduction

The scenario of massive star formation is still under debate. Theoretical studies of spherically symmetric collapsing cores predict specific solutions depending on their initial state (Whitworth & Summers 1985). Stable cores with little influence of external pressure evolve slowly and quasi-statically towards instability. Singular isothermal sphere (Shu 1977) and turbulent polytropic sphere (McKee & Tan 2003) models are proposed for high-mass star formation. Initially unstable cores evolve rapidly under the influence of external pressure. The model of global hierarchical collapse (Vázquez-Semadeni et al. 2019) considers cores and their parent clouds as nonequilibrium dynamic objects. The cores collapse with constant infall velocity before the protostar formation. After this, both quasi-static and unstable core models have the $r^{-0.5}$ velocity radial profile in the inner free fall region, while the envelope retains its initial velocity structure. The envelope density corresponds to the common r^{-2} profile in both models. To test theoretical scenarios, we need to know systematic velocity profiles in the envelope.

The spatial distribution of systematic velocity within a core can be determined by fitting model spectral maps into observed ones. Among molecular lines, dense gas tracers, the HCO^+ lines are the most sensitive to systematic motions (Yoo et al. 2018). However, the direct fitting of spectral maps is time-consuming and rarely used due to correlations between parameters, dependence on initial conditions and poor convergence. Recently, a method based on a preliminary set of model spectral maps (Pirogov & Zemlyanukha 2021) has been developed using principal component analysis (PCA) and the k-nearest neighbors method (kNN). Using a spherically symmetric model, radial profiles of infall velocity were obtained in the L1287 (Pirogov & Zemlyanukha 2021) and G268.42−0.85 cores (Pirogov et al. 2023). The derived power-law indices are different from free fall, implying that the cores are unstable and globally collapsing. To make general conclusions, it is important to expand the list of analyzed objects.

2 A sample of the MALT90 cores

The MALT90 survey (Jackson et al. 2013) is the largest database of high-mass clumps (over 2000 objects) observed in molecular lines in the 3 mm range and based on the ATLASGAL 870 μm dust continuum Galactic plane survey (Schuller et al. 2009). Among the MALT90 objects with notable HCO^+(1–0) emission (peak $T_a^* \gtrsim 1$ K) we selected 110 ones with asymmetric HCO^+(1–0) lines and/or absorption dips. In 20 cores, the HCO^+(1–0) lines possess dips with "blue" peaks exceeding the "red" one. The peaks of the $H^{13}CO^+$(1–0) and N_2H^+(1–0) lines of lower optical depth are close to the velocity of the HCO^+(1–0) dips, probably implying contraction. In this study

we present the results of analysis of five cores. The list of the sample cores is given in Table 1.

Table 1. The list of the sample cores. Kinematic distances are taken from Urquhart et al. (2022). Evolution statuses (Guzmán et al. 2015; Rathborne et al. 2016) are the following: H II region (H), protostellar core (A) and uncertain (U).

Source	l deg	b deg	RA(J2000) hh:mm:ss	Dec(J2000) $^o:':''$	D kpc	Evolution status	Associations with other sources
G012.418+00.506	12.419	0.507	18:10:51.1	−17:55:49.6	1.8	H	IRAS 18079−1756, EGO
G326.472+00.888	326.472	0.889	15:42:29.6	−53:58:26.7	2.5	U	
G328.567−00.535	328.568	−0.534	15:59:37.4	−53:45:51.7	2.9	H	IRAS 15557−5337, RCW99
G335.586−00.289	335.586	−0.289	16:30:58.7	−48:43:48.0	3.2	A	IRAS 16272−4837, SIRDC, EGO
G343.127−00.063	343.128	−0.063	16:58:17.5	−42:52:04.0	2.8	A	IRAS 16547−4247, EGO

The HCO^+(1–0) integrated intensity maps of the sample cores together with the Spitzer[1] and ATLASGAL maps are shown in Fig. 1. Four sources are associated with bright IRAS sources ($L_{\rm bol}$ are of the order of 10^4–10^5 $L_\odot$), three of them possess maser sources[2]. The masses of cores derived from the dust continuum lie in the range: 280–1200 $M_\odot$ (Csengeri et al. 2017; Lin et al. 2019). Values of dust temperatures vary in the range of 20–35 K (Urquhart et al. 2022). The G326.472 core with no embedded sources is probably at the earliest stage of evolution.

Table 2. Physical parameters of the MALT90 cores obtained from modeling: values of n_0, $V_{\rm turb}$ and $V_{\rm sys}$ in the central layer with the radius of 6.5×10^{-3} pc.

Object	$\log n_0$ [cm^{-3}]	α_n	$V_{\rm turb}$ km/s	$\alpha_{\rm turb}$	$V_{\rm sys}$ km/s	$\alpha_{\rm sys}$	$\log X$ (HCO^+)
G012.418+00.506	$9.0^{+0.1}_{-1.1}$	$2.5^{+0.1}_{-0.2}$	$3.2^{+3.8}_{-0.2}$	$0.38^{+0.02}_{-0.13}$	$-1.6^{+0.6}_{-0.5}$	$0.1^{+0.05}_{-0.05}$	$-9.8^{+0.3}_{-0.7}$
G326.472+00.888	$8.3^{+0.7}_{-0.4}$	$1.5^{+0.3}_{-0.1}$	$8.4^{+3}_{-0.9}$	$0.36^{+0.09}_{-0.06}$	$-1.6^{+0.4}_{-0.3}$	$0.1^{+0.05}_{-0.07}$	$-10.9^{+0.4}_{-0.4}$
G328.567−00.535	$9.1^{+0.1}_{-0.6}$	$2.0^{+0.1}_{-0.5}$	5^{+5}_{-1}	$0.33^{+0.22}_{-0.08}$	$-1.0^{+0.1}_{-1.0}$	$0.06^{+0.14}_{-0.03}$	$-10.3^{+0.3}_{-1.1}$
G335.586−00.289	$9.7^{+0.2}_{-1.0}$	$2.1^{+0.3}_{-0.6}$	$4.8^{+2.8}_{-1.8}$	$0.30^{+0.2}_{-0.05}$	$-1.6^{+0.6}_{-0.5}$	$0.1^{+0.1}_{-0.05}$	$-10.6^{+0.2}_{-0.6}$
G343.127−00.063	$8.7^{+0.8}_{-0.2}$	$2.0^{+0.3}_{-0.2}$	$10^{+0.1}_{-3.4}$	$0.45^{+0.01}_{-0.14}$	$-1.1^{+0.1}_{-0.9}$	$0.06^{+0.09}_{-0.06}$	$-9.9^{+0.3}_{-0.7}$

3 Results and discussion

The performed HCO^+(1–0) spectral maps were modeled using a spherically symmetric multi-layer model, where density n_0, turbulent $V_{\rm turb}$ and systematic $V_{\rm sys}$ velocities depend on radial distance as: $P_0/(1 + (r/R_0)^{\alpha_p})$ (see Appendix to Pirogov &

[1] https://irsa.ipac.caltech.edu/data/SPITZER/GLIMPSE/

[2] The maser sources positions are taken from https://maserdb.net database (Ladeyschikov et al. 2019)

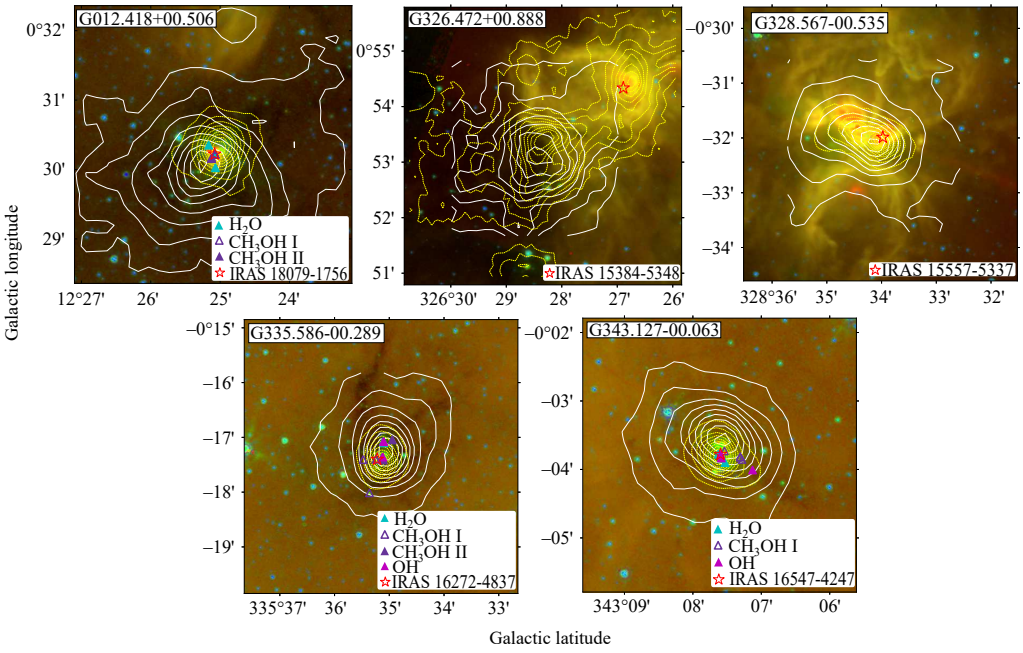

Fig. 1. Maps of the MALT90 sample cores. The colors represent the Spitzer data at 8 μm (red), 5.8 μm (green) and 3.6 μm (blue). The ATLASGAL data are shown by yellow dotted contours. The MALT90 HCO^+(1–0) integrated intensities are shown by white contours. The contours range from 10% to 90% of peak intensities.

Zemlyanukha 2021). The minimum of the error function between model and observed maps was found using the PCA and kNN methods, and the derived parameters are given in Table 2. Uncertainties were obtained from the analysis of the error projections function on the planes of different pairs of parameters (Pirogov & Zemlyanukha 2021; Pirogov et al. 2023).

Density profile power-law indices vary from -1.5 to -2.5. The G012.418 core has the sharpest density profile, the G326.472 core has the most shallow one. All the cores appear to be highly turbulent. Turbulent velocity profile indices vary from -0.3 to -0.45. Systematic velocities are negative corresponding to infall. Their profiles in all the cores are close to $r^{-0.1}$.

In the SEDIGISM survey (Schuller et al. 2021), the regions with the G012.418, G335.586 and G343.127 cores were observed. Analysis of the ^{13}CO(2–1) position-velocity profiles revealed the V-shape features (Fig. 3), which are signatures of accretion motions from surrounding gas to the cores located closer to the observer (e.g., Zhou et al. 2023). The fitting of model radial velocity profiles ($r^{-\alpha}$) with different α values shows that profiles with $\alpha \lesssim 0.5$ are preferable for the cores.

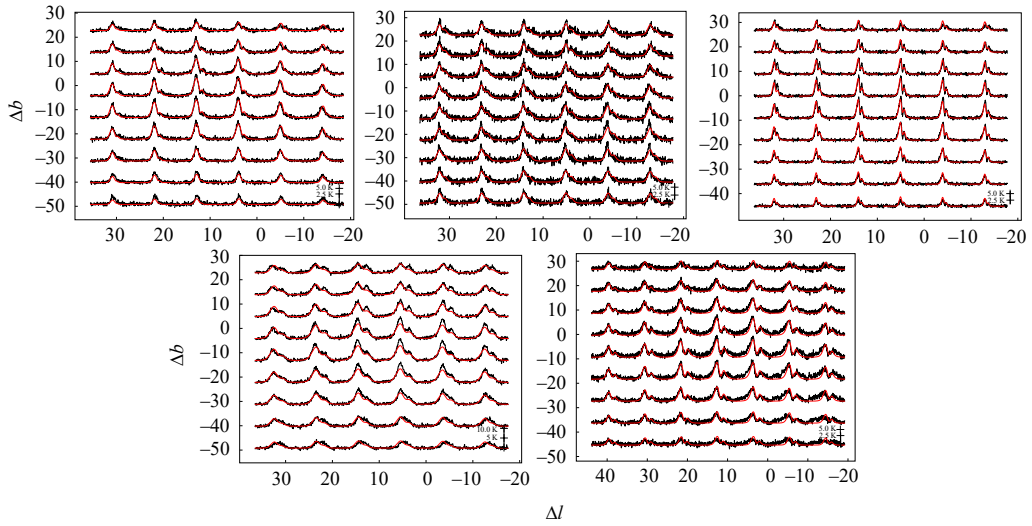

Fig. 2. The observed (black) and model (red) spectral maps of the sample cores in the HCO^+(1–0) line. The axes are the offsets relative to the coordinates from Table 1. Intensity scales are shown in the lower right corners of each panel. Velocity ranges (in km/s) are: [7...26], [−52...−29], [−54.5...−41] for G012.418, G326.472, G328.567, respectively (upper row) and [−54...−39],[−42...−20] for G335.586, G343.127, respectively (lower row).

4 Summary

We analyzed the HCO^+(1–0) spectral maps of five massive MALT90 cores associated with the regions of high-mass star formation at different stages of evolution. Using a spherically symmetric model and an algorithm for minimizing the error between model and observed spectral maps, radial profiles of n_0, $V_{\rm turb}$, $V_{\rm sys}$ are obtained. Densities in the cores decrease with radial distance with power-law indices from 1.5 to 2.5, turbulent velocities decrease with power-law indices from 0.3 to 0.45. Systematic (infall) velocity profiles are close to $r^{-0.1}$, which is different from what is expected for free fall. Analysis of position-velocity profiles from the ^{13}CO (2–1) SEDIGISM data revealed the V-shape features in three sample objects implying motions from surrounding gas to the cores. So the results support the scenario of globally contracting cores which interact with their surroundings.

Acknowledgements. This research has made use of the MALT90 Database available in the Australian Telescope Online Archive (http://atoa.atnf.csiro.au), and the SEDIGISM database (https://sedigism.mpifr-bonn.mpg.de) constructed by James Urquhart and hosted by the Max Planck Institute for Radio Astronomy.

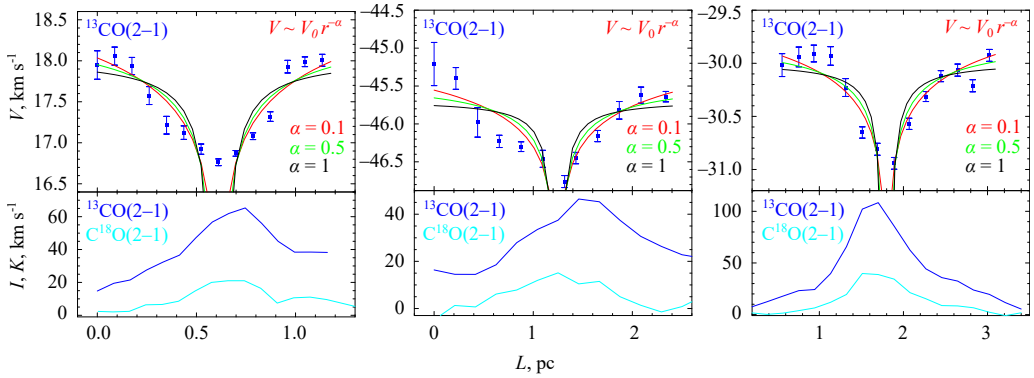

Fig. 3. The position-velocity profiles (upper panels) and the ^{13}CO (2–1) and C^{18}O (2–1) integrated intensity profiles (lower panels) across the G012.418 (left), G335.586 (center) and G343.127 (right) cores. Smooth curves of different colors correspond to the model radial velocity profiles.

Funding

The work is supported by the Russian Science Foundation grant No. 23-22-00139.

References

Csengeri T., Bontemps S., Wyrowski F., et al., 2017, Astronomy & Astrophysics, 601, id. A60
Guzmán A., Sanhueza P., Contreras Y., et al., 2015, Astrophysical Journal, 815, 2, id. 130
Jackson J., Rathborne J., Foster J., et al., 2013, Publ. Astron. Soc. Australia, 30, id. e057
Ladeyschikov D., Bayandina O., Sobolev A., 2019, Astronomical Journal, 158, 6, id. 233
Lin Y., Csengeri T., Wyrowski F., et al., 2019, Astronomy & Astrophysics, 631, id. A72
McKee C. and Tan J., 2003, Astrophysical Journal, 585, 2, p. 850
Pirogov L. and Zemlyanukha P., 2021, Astronomy Reports, 65, 2, p. 82
Pirogov L., Zemlyanukha P., Dombek E., et al., 2023, Astronomy Reports, 67, 12, p. 1355
Rathborne J., Whitaker J., Jackson J., et al., 2016, Publ. Astron. Soc. Australia, 33, id. e030
Schuller F., Menten K., Contreras Y., et al., 2009, Astronomy & Astrophysics, 504, 2, p. 415
Schuller F., Urquhart J., Csengeri T., et al., 2021, Monthly Notices of the Royal Astronomical Society, 500, 3, p. 3064
Shu F., 1977, Astrophysical Journal, 214, p. 488
Urquhart J., Wells M., Pillai T., et al., 2022, Monthly Notices of the Royal Astronomical Society, 510, 3, p. 3389
Vázquez-Semadeni E., Palau A., Ballesteros-Paredes J., et al., 2019, Monthly Notices of the Royal Astronomical Society, 490, 3, p. 3061
Whitworth A. and Summers D., 1985, Monthly Notices of the Royal Astronomical Society, 214, p. 1
Yoo H., Kim K., Cho J., et al., 2018, Astrophysical Journal Supplement, 235, 2, id. 31
Zhou J., Wyrowski F., Neupane S., et al., 2023, Astronomy & Astrophysics, 676, id. A69